Chinese Journal of Natural Medicines

Chinese agarwood petroleum ether extract suppressed gastric cancer progression *via* up-regulation of DNA damage-induced G_0/G_1 phase arrest and HO-1-mediated ferroptosis

Lishan Ouyang, Xuejiao Wei, Fei Wang, Huiming Huang, Xinyu Qiu, Zhuguo Wang, Peng Tan, Yufeng Gao, Ruoxin Zhang, Jun Li, Zhongdong Hu

Citation: Lishan Ouyang, Xuejiao Wei, Fei Wang, Huiming Huang, Xinyu Qiu, Zhuguo Wang, Peng Tan, Yufeng Gao, Ruoxin Zhang, Jun Li, Zhongdong Hu, Chinese agarwood petroleum ether extract suppressed gastric cancer progression *via* up-regulation of DNA damage-induced G_0/G_1 phase arrest and HO-1-mediated ferroptosis, Chinese Journal of Natural Medicines, 2025, 23(10), 1210-1220. doi: 10.1016/S1875-5364(25)60876-4.

View online: https://doi.org/10.1016/S1875-5364(25)60876-4

Wechat

Chinese Journal of Natural Medicines 23 (2025) 1210-1220

Contents lists available at ScienceDirect

Chinese Journal of Natural Medicines

journal homepage: www.cjnmcpu.com/

Original article

Chinese agarwood petroleum ether extract suppressed gastric cancer progression *via* up-regulation of DNA damage-induced G_0/G_1 phase arrest and HO-1-mediated ferroptosis

Lishan Ouyang[a,b,Δ], Xuejiao Wei[a,b,Δ], Fei Wang[a,b], Huiming Huang[a,b], Xinyu Qiu[a,b], Zhuguo Wang[a,b], Peng Tan[a,b], Yufeng Gao[a,b], Ruoxin Zhang[a,b], Jun Li[a], Zhongdong Hu[b,*]

[a] *School of Chinese Materia Medica, Beijing University of Chinese Medicine, Beijing 100029, China*
[b] *Modern Research Center for Traditional Chinese Medicine, Beijing Research Institute of Chinese Medicine, Beijing University of Chinese Medicine, Beijing 100029, China*

ARTICLE INFO

Article history:
Received 4 October 2024
Revised 27 December 2024
Accepted 3 January 2025
Available online 20 October 2025

Keywords:
Chinese agarwood petroleum ether extract (CAPEE)
Gastric cancer
G_0/G_1 phase arrest
Ferroptosis
DNA damage-p21-Cyclin D1/CDK4 signaling axis
HO-1

ABSTRACT

Gastric cancer (GC) is characterized by high morbidity and mortality rates. Chinese agarwood comprises the resin-containing wood of *Aquilaria sinensis* (Lour.) Gilg., traditionally utilized for treating asthma, cardiac ischemia, and tumors. However, comprehensive research regarding its anti-GC effects and underlying mechanisms remains limited. In this study, Chinese agarwood petroleum ether extract (CAPEE) demonstrated potent cytotoxicity against human GC cells, with half maximal inhibitory concentration (IC_{50}) values for AGS, HGC27, and MGC803 cells of 2.89, 2.46, and 2.37 μg·mL^{-1}, respectively, at 48 h. CAPEE significantly induced apoptosis in these GC cells, with B-cell lymphoma-2 (BCL-2) associated X protein (BAX)/BCL-2 antagonist killer 1 (BAK) likely mediating CAPEE-induced apoptosis. Furthermore, CAPEE induced G_0/G_1 phase cell cycle arrest in human GC cells *via* activation of the deoxyribonucleic acid (DNA) damage-p21-cyclin D1/cyclin-dependent kinase 4 (CDK4) signaling axis, and increased Fe^{2+}, lipid peroxides and reactive oxygen species (ROS) levels, thereby inducing ferroptosis. Ribonucleic acid (RNA) sequencing, real-time quantitative polymerase chain reaction (RT-qPCR), and Western blotting analyses revealed CAPEE-mediated upregulation of heme oxygenase-1 (HO-1) in human GC cells. RNA interference studies demonstrated that HO-1 knockdown reduced CAPEE sensitivity and inhibited CAPEE-induced ferroptosis in human GC cells. Additionally, CAPEE administration exhibited robust *in vivo* anti-GC activity without significant toxicity in nude mice while inhibiting tumor cell growth and promoting apoptosis in tumor tissues. These findings indicate that CAPEE suppresses human GC cell growth through upregulation of the DNA damage-p21-cyclin D1/CDK4 signaling axis and HO-1-mediated ferroptosis, suggesting its potential as a candidate drug for GC treatment.

1. Introduction

Gastric cancer (GC) represents the fifth most prevalent cancer in terms of morbidity and mortality in China. Globally, it ranks second only to lung cancer in mortality rates, presenting a significant threat to public health [1]. Current GC treatment modalities include conventional surgery, chemotherapy, targeted drug therapy, radiotherapy， and immunotherapy [2]. However, due to limitations in these treatment approaches, the therapeutic outcomes for GC remain suboptimal. Consequently, there is a critical need to investigate and develop novel anti-GC therapeutic agents. Research indicates that exploring traditional Chinese medicine for anti-GC compounds represents a promising strategy.

Chinese agarwood, derived from the resinous wood of *Aquilaria sinensis* (Lour.) Gilg., belongs to the Rafflesiaceae family. Traditional Chinese medicine recognizes its effectiveness in promoting qi circulation, alleviating pain, warming the body, and reducing vomiting. Contemporary pharmacological research has established multiple therapeutic properties of Chinese agarwood, including anti-inflammatory, antioxidant, and anti-tumor effects [3, 4]. Given that oxidative stress and inflammation are established mechanisms in cancer development [5], the anti-GC properties of Chinese agarwood align with both traditional medicine principles and modern research findings. Studies have identified sesquiterpenes and chromones as primary constituents of Chinese agarwood [6]. Moreover, methanol and ethanol extracts of Chinese agarwood have demonstrated significant cytotoxicity against various cancer cell lines, including colorectal, pancreatic, prostate, and breast cancers [5]. Research has shown that Chinese agarwood essential oil effectively inhibits the proliferation of breast cancer [7] and colorectal cancer cells [8]. Based on these findings, this study investigates the anti-GC effects of Chinese agarwood and its underlying mechanisms, aiming to identify potential therapeutic candidates and provide scientific evidence for im-

* Corresponding author.
E-mail address: zdhu@bucm.edu.cn
Δ These authors contributed equally to this work.

https://doi.org/10.1016/S1875-5364(25)60876-4

proving current diagnostic and therapeutic approaches for GC treatment.

Our findings demonstrate that Chinese agarwood petroleum ether extract (CAPEE) inhibited human GC cell growth, enhanced their apoptosis, arrested the cell cycle in the G_0/G_1 phase, and induced ferroptosis. The deoxyribonucleic acid (DNA) damage-p21-cyclin D1/cyclin-dependent kinase 4 (CDK4) pathway likely mediated CAPEE-induced cell cycle arrest in human GC cells. Iron accumulation resulting from heme oxygenase-1 (HO-1) activation potentially regulated CAPEE-induced ferroptosis in human GC cells. Furthermore, CAPEE demonstrated substantial anti-GC efficacy *in vivo*. These findings suggest CAPEE as a potential therapeutic agent for GC treatment.

2. Materials and methods

2.1. Reagents, antibodies, and drugs

Dulbecco's modified Eagle's medium (DMEM) (10–013-CV), Roswell Park Memorial Institute (RPMI-1640) (30–002-CI), and fetal bovine serum (FBS) (35–010-CV) were acquired from Corning Life Sciences (Steuben County, New York, USA). Deferoxamine (DFO) (HY-B0988), z-VAD-fmk (HY-16658B), *N*-acetylcysteine (NAC) (HY-B0215) and ferrostatin-1 (Fer-1) (HY-100579) were procured from MedChem Express (Monmouth Junction, New Jersey, USA). Methyl thiazolyl tetrazolium (MTT) powder (BN30793) was sourced from Biorigin (Beijing, China). BeyoClick™ 5-ethynyl-2'-deoxyuridine (EdU)-488 kit (C0071S), cell cycle detection kit (C1052), apoptosis detection kit (C1062L), DCFH-DA (S0033), and BDP 581/591 C11 (S0043) were obtained from Beyotime Biotechnology (Shanghai, China). Fe^{2+} assay kit (E-BC-K880-M) was purchased from Elabscience (Wuhan, China). Cell/Tissue total ribonucleic acid (RNA) isolation kit (RC101-01), all-in-one Q RT SuperMix (R333-01), and Taq Pro Universal SYBR quantitative polymerase chain reaction (qPCR) Master Mix (Q712-02) were acquired from Vazyme Biotech (Nanjing, China). *β*-Actin (sc-47778) and HO-1 (sc-13696) antibodies were purchased from Santa Cruz Biotechnology (Santa Cruz, CA, USA). Cyclin D1 (2978), p21 (2947), CDK4 (12790), and γ-H2AX (9718) antibodies were obtained from Cell Signaling Technology (Danvers, MA, USA).

2.2. Preparation of CAPEE

Chinese agarwood, the resinous wood of *Aquilaria sinensis* (Lour.) Gilg, was collected in Hainan Province, China, and identified by the Professor Pengfei Tu of Peking University. The sample was preserved at the Modern Research Center for Traditional Chinese Medicine, Beijing University of Chinese Medicine, Beijing, China, with the specimen sequence number 19101801. A quantity of 10.0 kg of Chinese agarwood was weighed, pulverized, and extracted through refluxing with 95% ethanol twice, each extraction continuing for 2 h, followed by a 2-h reflux with 70% ethanol. The extracts were combined, and the solvents were recovered through decompression. The resulting extracts were subsequently dispersed in water and extracted with petroleum ether, yielding 84.9 g of CAPEE [9]. Subsequently, CAPEE was dissolved in DMSO to create 4 and 8 $mg \cdot mL^{-1}$ stock solutions and stored at −20 °C for short-term use. Previous research has established that CAPEE primarily comprises 26 sesquiterpenes [10].

2.3. Cell culture

Human GC cells (AGS, HGC27, and MGC803) and human normal gastric epithelial cells (GES-1) were obtained from the Cell Culture Center of the Institute of Basic Medical Sciences of the Chinese Academy of Medical Sciences. AGS and HGC27 cells were maintained in the RPMI-1640 medium, while MGC803 and GES-1 cells in DMEM. Both media contained 10% FBS and 1% penicillin-streptomycin. Cells were cultured at 37 °C with 5% CO_2.

2.4. Cell viability assay

Human GC cells (2×10^3/well) were seeded into 96-well plates. After 24 h of culture, cells were treated with CAPEE at various concentrations. Five replicate wells were established per concentration. Inhibitors were applied at the following concentrations: z-VAD-fmk: 5 $\mu mol \cdot L^{-1}$; DFO: 10 $\mu mol \cdot L^{-1}$; NAC: 50 $\mu mol \cdot L^{-1}$; Fer-1: 25 $\mu mol \cdot L^{-1}$. Post-treatment, 5 $\mu g \cdot mL^{-1}$ MTT solution (100 μL) was added to each well. Following 4 h of incubation, the MTT mixture was aspirated, DMSO (150 μL) was added to each well, and absorbance was measured at 490 nm.

2.5. EdU cell proliferation assay

Human GC cells (4×10^5/well) were seeded in 6-well plates and cultured for 24 h, followed by 48 h of treatment with 0 or 4 $\mu g \cdot mL^{-1}$ CAPEE. Three replicate wells were established per concentration. Following BeyoClick™ EdU-488 kit protocols, EdU labeling, fixation, washing, permeabilization, and click reactions were performed. The samples were double-labeled with Alexa Fluor 488 and Hoechst 33342, and images were captured using a fluorescence microscope.

2.6. Cell colony formation experiment

Human GC cells (300/well) were seeded into 6-well plates and cultured for 24 h. Subsequently, 1 $\mu g \cdot mL^{-1}$ CAPEE was added, with medium changes every 3 days. Three replicate wells were established per concentration. After 10 days of treatment, cells were washed with phosphate-buffered saline (PBS), fixed with 4% paraformaldehyde for 15 min, stained with 0.1% crystal violet for 30 min, washed with PBS, photographed, and counted.

2.7. Flow cytometry

Human GC cells (4×10^5/well) were seeded in 6-well plates and cultured for 24 h, followed by 48 h of treatment with 0, 4, or 8 $\mu g \cdot mL^{-1}$ CAPEE. Three replicate wells were established per concentration. For cell cycle detection, cells were starved for 24 h after wall adherence. For reactive oxygen species (ROS) level measurement, 50 $\mu g \cdot mL^{-1}$ Rosup served as the positive control. Relevant indices were determined using corresponding kits. For apoptosis detection, cells were stained with Annexin V-fluorescein isothiocyanate (FITC) and propidium iodide (PI) in darkness. For cell cycle evaluation, cells were fixed with 95% ethanol and stained with PI in darkness. For ROS detection, DCFH-DA was used for light-protected staining, and for lipid peroxide detection, a lipid peroxidation probe (BDP 581/591 C11) was applied under light-protected conditions. All indicators were analyzed *via* flow cytometry at appropriate wavelengths.

2.8. Comet assay

Human GC cells (4×10^5/well) were cultured in 6-well plates for 24 h. Subsequently, cells were treated with 0 or 4 $\mu g \cdot mL^{-1}$ CAPEE for 24 h. Three replicate wells were established per concentration. DNA damage was assessed according to kit instructions. A high-melting point gel layer was prepared before creating the single-cell suspension (1×10^6 cells/mL). Cells were combined with low-melting-point gel and applied dropwise to the high-melting-point gel. After solidification, another low-melting-

point gel layer was added dropwise. The samples underwent lysis, electrophoresis, PI staining, and imaging using a fluorescence microscope.

2.9. Detection of Fe^{2+} levels

Human GC cells (2×10^5/well) were seeded into 6-well plates, cultured for 24 h, and treated with 0, 4, or 8 μg·mL^{-1} CAPEE for 48 h. Three replicate wells were established per concentration. Intracellular Fe^{2+} ions were labeled using the cell total iron colorimetric assay kit. Following dark incubation at 37 °C, absorbance was measured at 593 nm.

2.10. RNA sequencing

Human GC HGC27 cells were seeded into 6-cm dishes, and at 60% confluence, 0 or 8 μg·mL^{-1} CAPEE was administered for 24 h. Three replicate wells were established per concentration. Following PBS washing, cells underwent lysis with RNA-Solv reagent on ice for 5 min. The obtained samples were sequenced at Shanghai Biotechnology Corporation. Subsequently, Gene Ontology (GO) and Kyoto Encyclopedia of Genes and Genomes (KEGG) analyses were conducted in R 4.2.2 using the clusterProfiler package.

2.11. Real-time qPCR (RT-qPCR)

Human GC cells were inoculated into 6-cm dishes and incubated for 24 h, followed by treatment with either 0 or 8 μg·mL^{-1} CAPEE for an additional 24 h. Total RNA was extracted using a commercial RNA isolation kit according to the manufacturer's instructions. RNA concentration and purity were determined using a NanoDrop 2000 spectrophotometer. First-strand complementary DNA (cDNA) was synthesized from total RNA *via* reverse transcription. RT-qPCR was then performed in 20 μL reaction volumes containing 10 μL of 2 × Taq Pro Universal SYBR qPCR Master Mix, 4 μL of cDNA template, 0.4 μL each of forward and reverse primers (10 μmol·L^{-1}), and 4 μL of RNase-free ddH_2O. Each treatment condition was assessed in five technical replicates. The qPCR cycling protocol consisted of an initial denaturation at 94 °C for 30 sec, followed by 40–45 amplification cycles of 94 °C for 5 sec and 60 °C for 15 seconds. Primer sequences used in the analysis are listed below:

p21 Forward primer: 5'-TGCCCAAGCTCTACCTTCC-3',

p21 Reverse primer: 5'-CAGGTCCACATGGTCTTCCT-3';

HO-1 Forward primer: 5'-AAGACTGCGTTCCTGCTCAAC-3',

HO-1 Reverse primer: 5'-AAAGCCCTACAGCAACTGTCG-3';

Glyceraldehyde-3-phosphate dehydrogenase (GAPDH) forward primer: 5'-CAGTGCCAGCCTCGTCTCAT-3',

GAPDH reverse primer: 5'-AGGGGCCATCCACAGTCTTC-3'.

2.12. Western blotting assay

Human GC cells were treated with varying doses of CAPEE for 48 h. Following lysis on ice using pre-prepared cell lysis solution, the cells underwent heating at 98 °C for 10 min for protein denaturation and subsequent storage at −40 °C. The samples were then subjected to loading, electrophoresis, electrotransfer, blocking, antibody incubation, and development. The experimental procedure was repeated three times to obtain consistent results for target protein expression changes. The cell lysate preparation methods and detailed experimental procedures were described previously [11,12].

2.13. RNA interference

Human GC cells were transfected upon reaching 70%–90% confluency in 6-well plates. The procedure involved adding Opti-MEM (125 μL) to Lipofectamine 3000 reagent (3.75 μL) per well for liposome dilution; Opti-MEM (250 μL) was combined with small interfering RNA (siRNA) reagent (5 μg) and P3000 reagent (10 μL) for DNA dilution. A mixture of 125 μL diluted liposome solution and 125 μL diluted DNA was incubated at ambient temperature for 10–15 min, followed by 48 h of culture. Transfection efficiency was evaluated through the Western blotting assay. The siRNA sequences used were as follows.

Negative control (NC): 5'-UUCUCCGAACGUGUCACGUTT-3',

HO-1: 5'-AAGCCACACAGCACUAUGUAA-3'.

2.14. Nude mouse xenograft tumor model

Male BALB/c nude mice (4–5 weeks old) were obtained from Beijing Vital River Laboratory Animal Technology Co., Ltd. and maintained in SPF-grade conditions at 23–27 °C, 49%–51% relative humidity, with a 12-h/12-h light/dark cycle. The mice received sterilized feed and double-distilled water. Each nude mouse received a subcutaneous injection of human GC HGC27 cells (3×10^6) beneath the right forelimb. Once tumor volume reached 100–200 mm^3, the animals were divided into the following groups (n = 9 mice/group): blank control group (double-distilled water solution containing 2.5% Tween 80, once/day, i.g.), CAPEE-treated group (200 mg·kg^{-1}, once/day, i.g.), and 5-FU-positive group (30 mg·kg^{-1}, once/2 days, i.p.). Daily monitoring included observation of mouse condition, body weight, and tumor volume (V = length × width^2/2). Following drug administration, samples were collected, and the major organs and tumor tissues were preserved in 4% paraformaldehyde for hematoxylin and eosin (H&E) staining and immunohistochemical analysis (Animal experimentation ethics number: BUCM-4-2021031603-1072).

2.15. H&E staining and immunohistochemical analysis

The fixed major organs and tumor tissues underwent gradient dehydration, transparent treatment, and embedding to generate tissue section samples for subsequent staining. H&E, terminal deoxynucleotidyl transferase-mediated dUTP nick end labeling (TUNEL), and immunohistochemistry staining for Ki67, PCNA, p21, and HO-1 were conducted according to previously described methods [13].

2.16. Statistical analysis

Statistical analysis and plotting were performed using GraphPad Prism 9.0 software, with data expressed as mean ± SD. Between-group differences were evaluated using t-tests, with $P < 0.05$ indicating statistical significance.

3. Results

3.1. CAPEE suppressed human GC cell proliferation

AGS, HGC27, and MGC803 cells were treated with CAPEE at concentrations of 0, 1, 2, 3, or 4 μg·mL^{-1}, and cell proliferation was assessed using MTT assay. Results demonstrated that CAPEE significantly inhibited human GC cell proliferation in both dose- and time-dependent manner. The half maximal inhibitory concentration (IC_{50}) values at 48 h for CAPEE in AGS, HGC27, and MGC803 cells were 2.89, 2.46, and 2.37 μg·mL^{-1}, respectively (Fig. 1A). EdU cell proliferation assays revealed that CAPEE markedly decreased proliferation rates in AGS, HGC27, and MGC803 cells (Fig. 1B). Additionally, CAPEE inhibited colony formation in these cell lines (Fig. 1C), indicating its anti-proliferative effect on human GC cells. Notably, CAPEE exhibited significantly lower cytotoxicity toward GES-1 compared to human GC

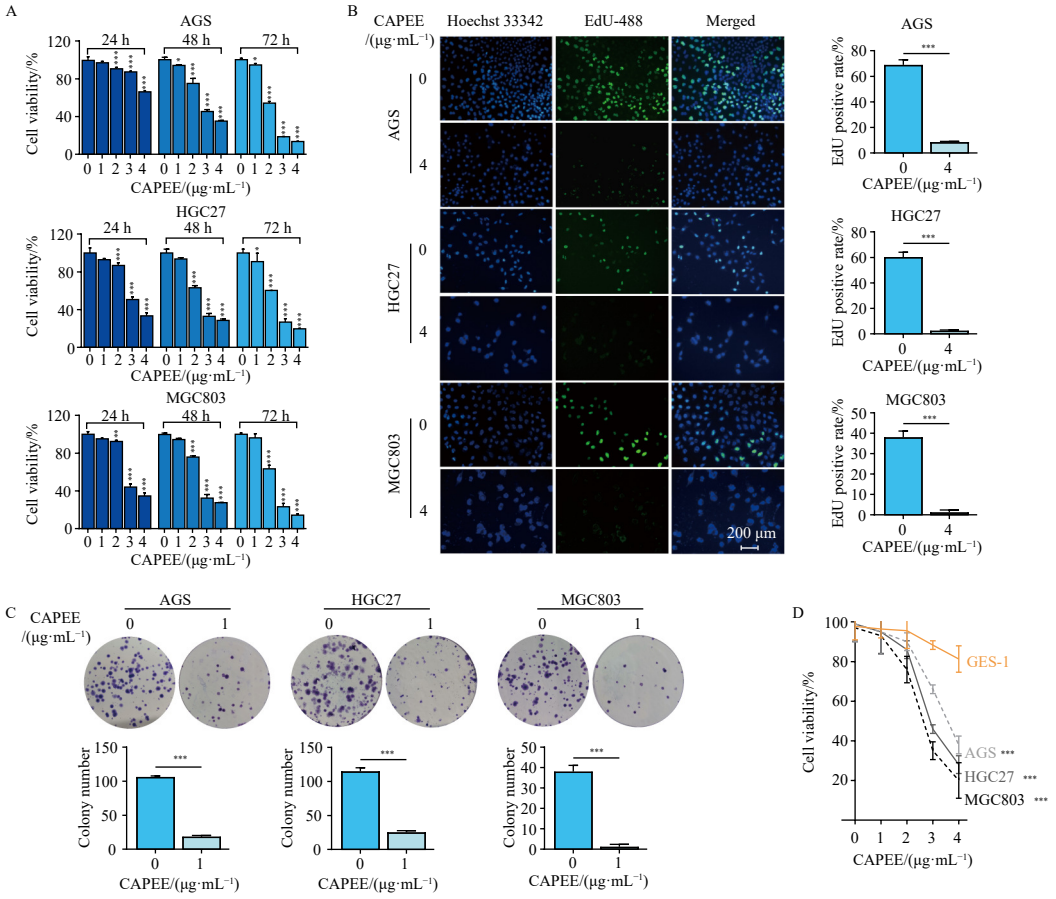

Fig. 1 CAPEE suppresses the proliferation of human GC cell lines AGS, HGC27, and MGC803. (A) Cell viability was assessed by MTT assay following treatment with increasing concentrations of CAPEE (0, 1, 2, 3, or 4 μg·mL^{-1}) for 24, 48, and 72 h in AGS, HGC27, and MGC803 cells (n = 3). (B) AGS, HGC-27, and MGC803 cells were exposed to 48 h of 0 or 4 μg·mL^{-1} CAPEE treatment. BeyoClick™ EdU-488 was added for cell labeling, and photographs were taken under a fluorescence microscope (n = 3). Left panel: representative images (× 200); right panel: EdU-positive cell proportion. (C) AGS, HGC27, and MGC803 cells were exposed to 10 d of 0 or 1 μg·mL^{-1} CAPEE treatment to observe colony formation (n = 3). Upper panel: representative images; lower panel: quantitative data. (D) 0, 1, 2, 3, or 4 μg·mL^{-1} CAPEE was added to treat human gastric epithelial GES-1 cells and AGS, HGC27, and MGC803 cells for 48 h, and viability was determined using the MTT assay (n = 3). The results were expressed as mean ± SD. $^{*}P$ < 0.05, $^{**}P$ < 0.01, and $^{***}P$ < 0.001.

cells, demonstrating selective specificity for human GC cells (Fig. 1D). These findings confirm that CAPEE effectively suppresses the proliferation of AGS, HGC27, and MGC803 cells.

3.2. CAPEE triggered apoptosis of human GC cells

Flow cytometry analysis with an Annexin V-FITC/PI dual probe was utilized to measure human GC cell apoptosis. The results demonstrated that CAPEE induced apoptosis in AGS, HGC27, and MGC803 cells in a dose-dependent manner (Fig. 2A). The apoptosis inhibitor z-VAD-fmk effectively suppresses apoptotic processes [14]. Following apoptosis inhibition by z-VAD-fmk, human GC cells exhibited reduced sensitivity to CAPEE (Fig. 2B). These findings indicate that CAPEE induced apoptosis in human GC cells. The proapoptotic proteins B-cell lymphoma-2 (BCL-2) associated X protein (BAX) and BCL-2 antagonist killer 1 (BAK) counteract BCL-2-mediated apoptotic escape [15]. The simultaneous knockout of BAX and BAK reduced CAPEE sensitivity in human GC HGC27 cells (Fig. 2C), indicating potential BAX/BAK involvement in CAPEE-induced human GC cell apoptosis.

3.3. CAPEE induced G_0/G_1 phase blockade of human GC cells by activating the DNA damage-p21-cyclin D1/CDK4 signaling axis

Human GC AGS, HGC27, and MGC803 cells were treated with CAPEE at concentrations of 0 or 4 μg·mL^{-1}. Flow cytometry analysis revealed that CAPEE administration induced cell cycle arrest in the G_0/G_1 phase of human GC cells (Fig. 3A). Transcriptome sequencing was performed to elucidate the molecular mechanism underlying CAPEE's inhibition of human GC cell growth. The analysis revealed upregulation of the gene *CDKN1A*, which corresponds to p21, in CAPEE-treated human GC cells. RT-qPCR confirmed increased *p21* mRNA levels in human GC cells following CAPEE treatment (Fig. 3B). Immunoblotting analysis demonstrated elevated p21 protein levels in CAPEE-treated human GC cells (Fig. 3C). Conversely, CAPEE treatment decreased cyclin D1 and CDK4 protein expression in human GC AGS, HGC27, and MGC803 cells (Fig. 3C). An investigation of the mechanism behind CAPEE-mediated p21 upregulation revealed DNA damage in human GC AGS, HGC27, and MGC803 cells, as demonstrated by comet assay (Fig. 3D). Additionally, immunoblotting showed increased expression of γ-H2AX protein, a DNA damage marker, in human GC cells (Fig. 3C). These findings indicate that CAPEE-induced DNA damage activates the p21-cyclin D1/CDK4 signaling axis, resulting in G_0/G_1 phase cell cycle arrest.

3.4. CAPEE induced human GC cell ferroptosis

Transcriptome sequencing analysis indicated that ferroptosis regulation might mediate the anti-GC efficacy of CAPEE (Supplementary Fig. S1). Fe^{2+} levels significantly increased within human GC AGS, HGC27, and MGC803 cells following CAPEE administration (Fig. 4A). Flow cytometry analysis revealed that ROS levels increased substantially in human GC AGS, HGC27, and MGC803 cells after CAPEE treatment, with the increase comparable to that induced by the positive control drug Rosup (Fig. 4B).

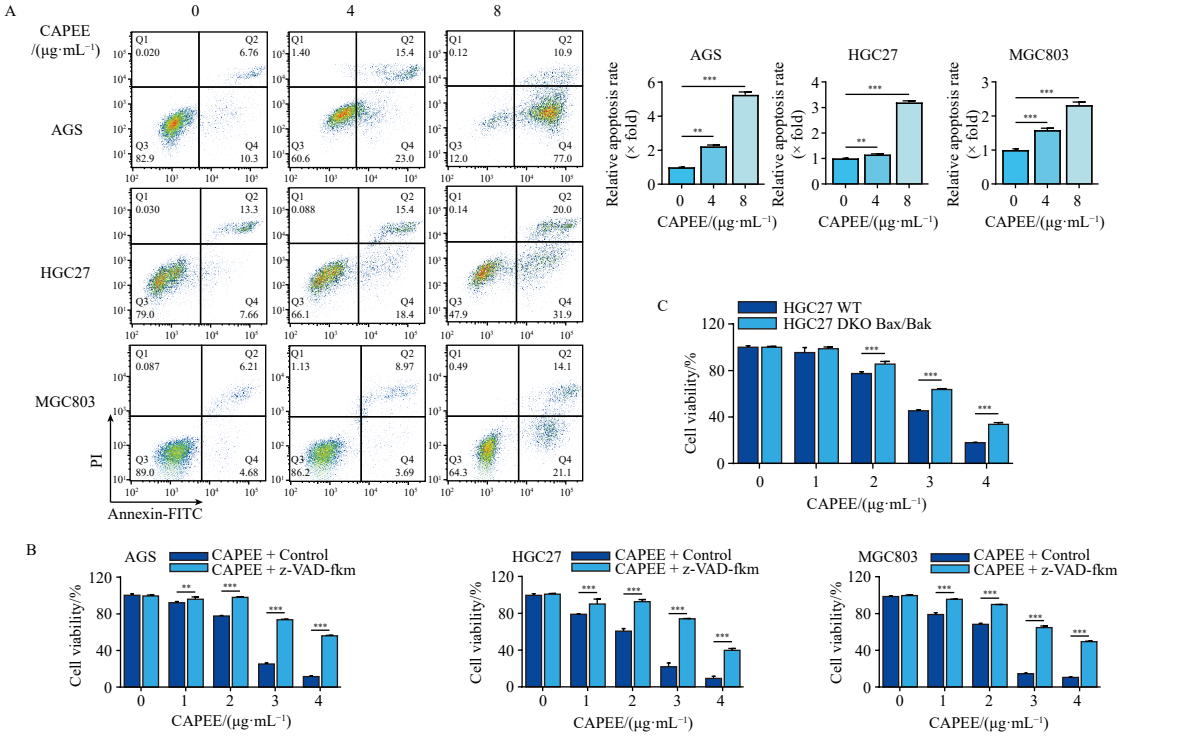

Fig. 2 CAPEE triggers the apoptosis of human GC cell lines AGS, HGC27, and MGC803. (A) AGS, HGC27, and MGC803 cells were exposed to 0, 4, and 8 μg·mL^{-1} CAPEE for 48 h. Flow cytometry was conducted to detect apoptosis (n = 3). Left panel: representative images; right panel: quantitative data. (B) CAPEE co-administered with z-VAD-fmk (5 μmol·L^{-1}) was used for 72 h of AGS, HGC27, and MGC803 cells treatment. MTT assay was performed to measure cell viability (n = 3). (C) BAX$^{-/-}$ BAK$^{-/-}$ HGC27 cells and wild-type HGC27 cells were exposed to 0, 1, 2, 3, or 4 μg·mL^{-1} CAPEE treatment. Cell viability was assessed by MTT assay (n = 3). The results were expressed as mean ± SD. $^{*}P$ < 0.05, $^{**}P$ < 0.01, and $^{***}P$ < 0.001.

Moreover, lipid peroxide levels increased significantly within GC cells following CAPEE administration (Fig. 4C). DFO, a ferric ion chelator, effectively sequesters free intracellular ferric ions [16]. NAC functions as a scavenger of ROS generated during oxidative stress [17]. Fer-1 reduces lipid peroxide formation [18]. The inhibition of ferroptosis through DFO, NAC, or Fer-1 diminished CAPEE sensitivity in human GC cells (Fig. 4D). These findings demonstrate that CAPEE induced ferroptosis in human GC cells.

3.5. HO-1 participated in inducing human GC cell ferroptosis by CAPEE

Transcriptome sequencing revealed that HO-1 expression increased significantly in HGC27 cells following CAPEE exposure (Fig. 5A). RT-qPCR results confirmed that CAPEE administration substantially elevated the mRNA level of *HO-1* in human GC AGS, HGC27, and MGC803 cells (Fig. 5B). Immunoblotting assay demonstrated that HO-1 protein expression notably increased within human GC AGS, HGC27, and MGC803 cells after CAPEE administration (Fig. 5C). Subsequently, RNA interference technology was employed to investigate HO-1's role in CAPEE's anti-GC effect. Immunoblotting experiments showed that siRNA targeting HO-1 significantly reduced HO-1 expression levels within human GC AGS, HGC27, and MGC803 cells (Fig. 5D). As CAPEE concentration increased, human GC cell viability in the siNC group decreased significantly, while the siHO-1 group exhibited a significantly lower cell proliferation inhibition rate compared to the siNC group (Fig. 5E), indicating that HO-1 knockdown reduced CAPEE sensitivity in human GC cells. HO-1 knockdown significantly diminished CAPEE-induced Fe^{2+} level elevation in AGS, HGC27, and MGC803 cells (Fig. 5F). Moreover, HO-1 knockdown significantly decreased CAPEE-mediated ROS content elevation in AGS, HGC27, and MGC803 cells (Fig. 5G). Furthermore, HO-1 expression inhibition significantly reduced CAPEE's ability to increase lipid peroxidation levels within AGS, HGC27, and MGC803 cells (Fig. 5H). These findings indicate that HO-1 up-regulation is associated with CAPEE-induced ferroptosis in human GC cells.

3.6. CAPEE treatment inhibited the tumorigenesis of human GC cells within nude mice

To evaluate *in vivo* anti-GC effect of CAPEE, a nude mouse xenograft tumor model was established using human GC HGC27 cells. CAPEE administration significantly inhibited tumor development and reduced tumor weight in thexenograft model (Figs. 6A and 6B). Furthermore, CAPEE administration did not notably affect mouse body weight, whereas mice in the 5-FU-positive drug group exhibited some degree of weight loss (Fig. 6C). H&E staining analysis demonstrated that CAPEE treatment caused no substantial damage to major organ tissues, including the mouse liver, heart, spleen, kidneys or lungs (Fig. 6D). The number of Ki67-positive and PCNA-positive cells in the CAPEE-treated group decreased significantly compared to the control group (Fig. 6E), indicating that CAPEE inhibited tumor tissue proliferation. Moreover, TUNEL staining results demonstrated that CAPEE induced apoptosis in mouse tumor tissue cells (Fig. 6E). The expression of p21 and HO-1 in the CAPEE-treated group increased markedly compared to the control group (Fig. 6E), consistent with the *in vitro* cellular experimental findings. These results demonstrate that CAPEE exhibits effective *in vivo* anti-GC activity.

4. Discussion

Chinese agarwood, a valuable medicinal material with extensive historical significance, has been utilized globally for centuries in treating various ailments. In ancient India and Egypt, agarwood incense served as a primary method for mental purification and tranquility [19]. Traditional Arabic medicine employs Chinese agarwood for treating neurodegenerative diseases and digestive disorders, recognizing its calming and sedative effects [20]. In traditional Chinese medicine, Chinese agarwood serves as an essential remedy for qi regulation, pain management,di-

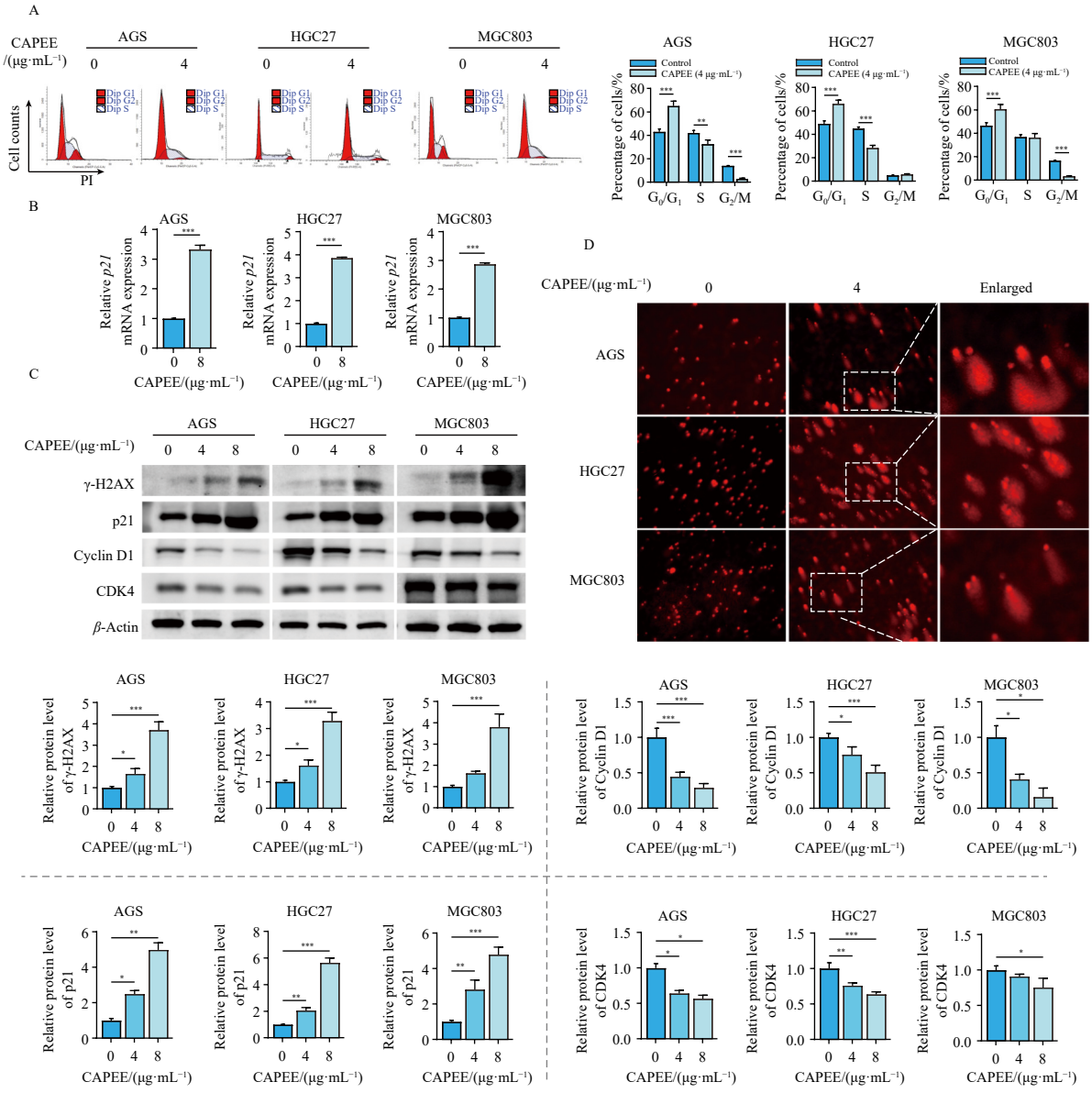

Fig. 3 CAPEE induces G_0/G_1 cell cycle arrest in human GC cells through DNA damage and regulation of the p21–Cyclin D1/CDK4 signaling pathway. (A) AGS, HGC27, and MGC803 cells were exposed to 48 h of 0 or 4 μg·mL^{-1} CAPEE treatment, while cell cycle distribution was evaluated through flow cytometry assay (n = 3). Left panel: representative images; right panel: quantitative data. (B) AGS, HGC27, and MGC803 cells were exposed to 24 h of 0 or 8 μg·mL^{-1} CAPEE treatment. *p21* mRNA levels in the cells were measured through qRT-PCR (n = 3). (C) AGS, HGC27, and MGC803 cells were exposed to 48 h of 0, 4, and 8 μg·mL^{-1} CAPEE treatment. Protein levels of γ-H2AX, p21, Cyclin D1, and CDK4 were detected by Western blotting analysis (n = 3). Upper panel: representative images; lower panel: quantitative data. (D) AGS, HGC27, and MGC803 cells were exposed to 24 h of 0 or 4 μg·mL^{-1} CAPEE treatment. DNA damage was detected using the comet assay. The results were expressed as mean ± SD. $^{*}P < 0.05$, $^{**}P < 0.01$, and $^{***}P < 0.001$.

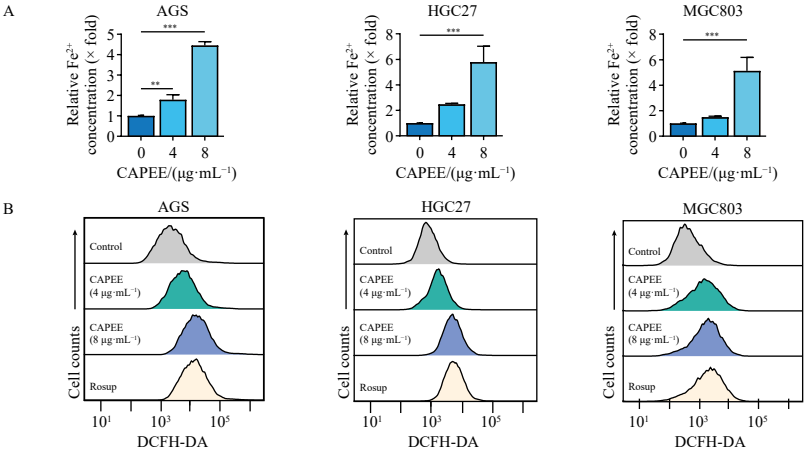

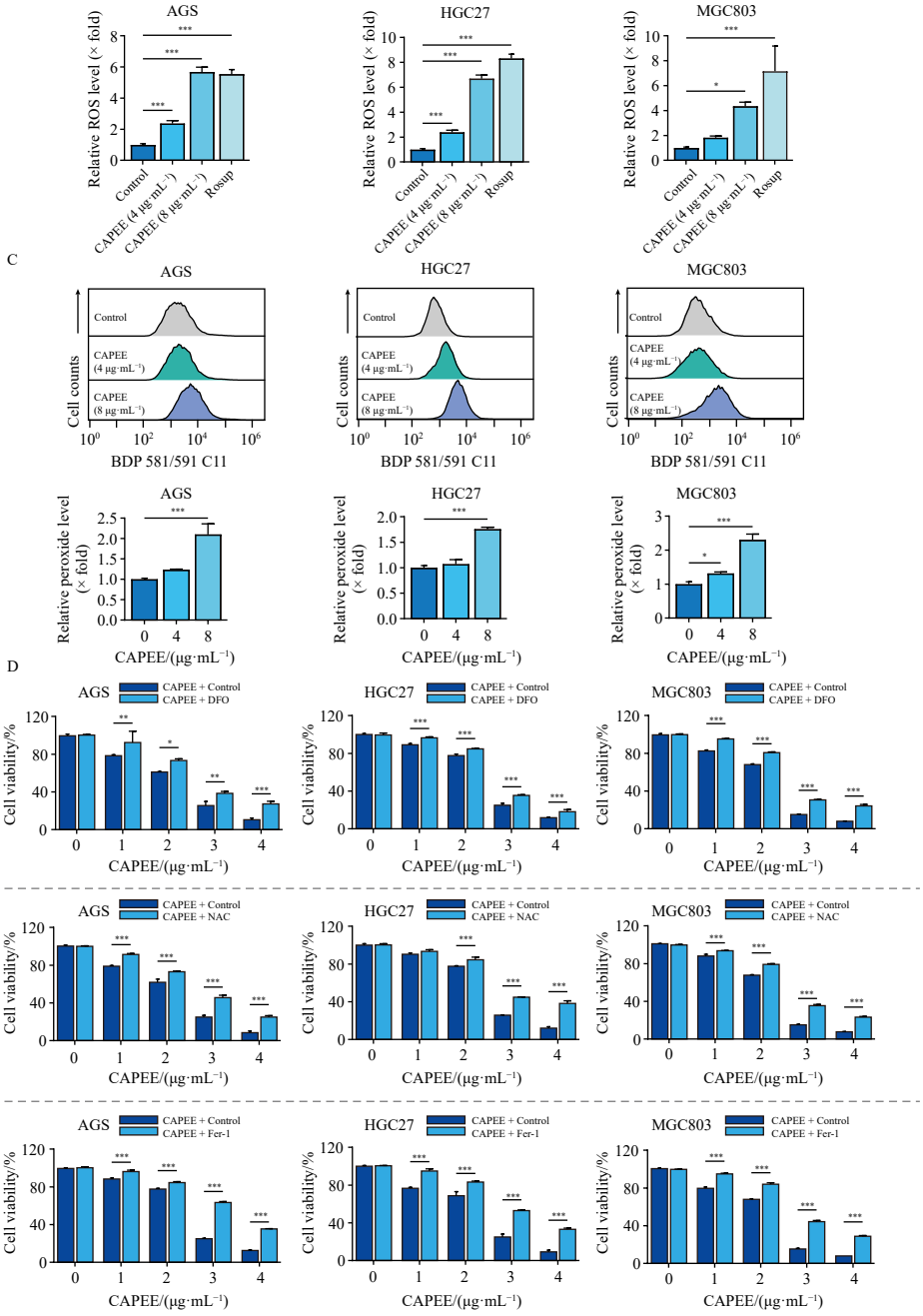

Fig. 4 CAPEE induces ferroptosis in human GC cell lines AGS, HGC27, and MGC803. AGS, HGC-27, and MGC803 cells were exposed to 48 h of 0, 4, or 8 μg·mL^{-1} CAPEE treatment unless otherwise indicated. (A) Intracellular Fe^{2+} levels were quantified to assess iron accumulation following CAPEE treatment (n = 3). (B) Intracellular ROS levels were measured through flow cytometry (n = 3). Upper panel: representative images; lower panel: quantitative data. (C) Lipid peroxidation was assessed by flow cytometry (n = 3). Upper panel: representative images; lower panel: quantitative data. (D) CAPEE was co-administered with DFO (10 μmol·L^{-1}), NAC (50 μmol·L^{-1}), and Fer-1 (25 μmol·L^{-1}) for 72 h. Cell viability was determined using the MTT assay (n = 3). The results were expressed as mean ± SD. $^{*}P < 0.05$, $^{**}P < 0.01$, and $^{***}P < 0.001$.

gestive enhancement, anti-emetic effects, and asthma treatment [21]. Contemporary pharmacological research has demonstrated that Chinese agarwood exhibits multiple biological activities, including anti-bacterial, anti-inflammatory, sedative, hypnotic, digestive, anti-depressant, and anti-tumor properties [4]. The aromatic composition of Chinese agarwood primarily comprises sesquiterpenes and 2-(2-phenylethyl)-chromones, with sesquiterpenes displaying greater variation in both fragrance and biological activity. Research has identified and characterized more than 200 varieties of sesquiterpenes and their derivatives from Chinese agarwood [4, 22–25]. Studies indicate that *Aquilaria crassna* essential oil extract significantly reduces the survival rate of human breast cancer MCF-7 cells [25] and human colorectal cancer HCT116 cells. The extract also demonstrates inhibitory effects on colorectal cancer HCT116 cell growth in subcutaneous tumors of nude mice. Toxicological studies reveal that the LD_{50} of the extract exceeds 2000 mg·kg^{-1}. The essential oil treatment group showed no significant variations in food and water intake, weight changes,hematological and biochemical parameters, relative organ weight, or histopathological findings compared to controls [8]. Both *in vitro* and *in vivo* toxicity analyses of various agarwood plant components confirm their safety at tested doses [5]. Furthermore, *β*-caryophyllene, isolated from *Aquilaria crassna* essential oil extract, demonstrates inhibitory effects on colorectal cancer cell proliferation and migration while inducing apoptosis [26]. Aquilariperoxide A, a diterpene dimer present in Chinese agarwood, significantly inhibits human cancer cell proliferation and migration while suppressing epithelial-mesenchymal transition [27]. Considering Chinese agarwood's extensive medicinal history, demonstrated clinical efficacy, and established safety pro-

file, particularly regarding its sesquiterpene components with notable anti-tumor properties, CAPEE shows promise for clinical applications with potentially enhanced therapeutic effects. As a sesquiterpene-enriched extract of Chinese agarwood, CAPEE demonstrates significant potential against GC and merits further investigation.

Apoptosis functions as a crucial mechanism for cellular population regulation, tissue homeostasis maintenance, and elimination of potentially harmful cells. The induction of tumor cell apoptosis establishes equilibrium between cell proliferation and death rates, thereby inhibiting tumor growth [28]. Apoptotic processes can be initiated through intracellular or extracellular signaling pathways. The regulation of endogenous apoptosis primarily involves mitochondrial processes and the activation of proapoptotic proteins, includingBAK and BAX [29]. BCL-2 effectively inhibits the mitochondrial apoptotic pathway [30]. BAX and BAK counteract BCL-2-mediated apoptotic escape [15]. The experimental results demonstrate that CAPEE significantly induced apoptosis in human GC AGS, HGC27, and MGC803 cells, while the double knockout of BAX and BAK reduced CAPEE sensitivity in human GC cells. These findings suggest that the mitochondrial pathway may be involved in CAPEE-induced apoptosis of human GC cells.

Several anti-tumor drugs approved by the FDA for clinical use effectively block cancer cell cycle in G_0/G_1 phase [31]. Similarly, numerous natural products derived from traditional Chinese medicine demonstrate the ability to arrest cancer cell cycle in

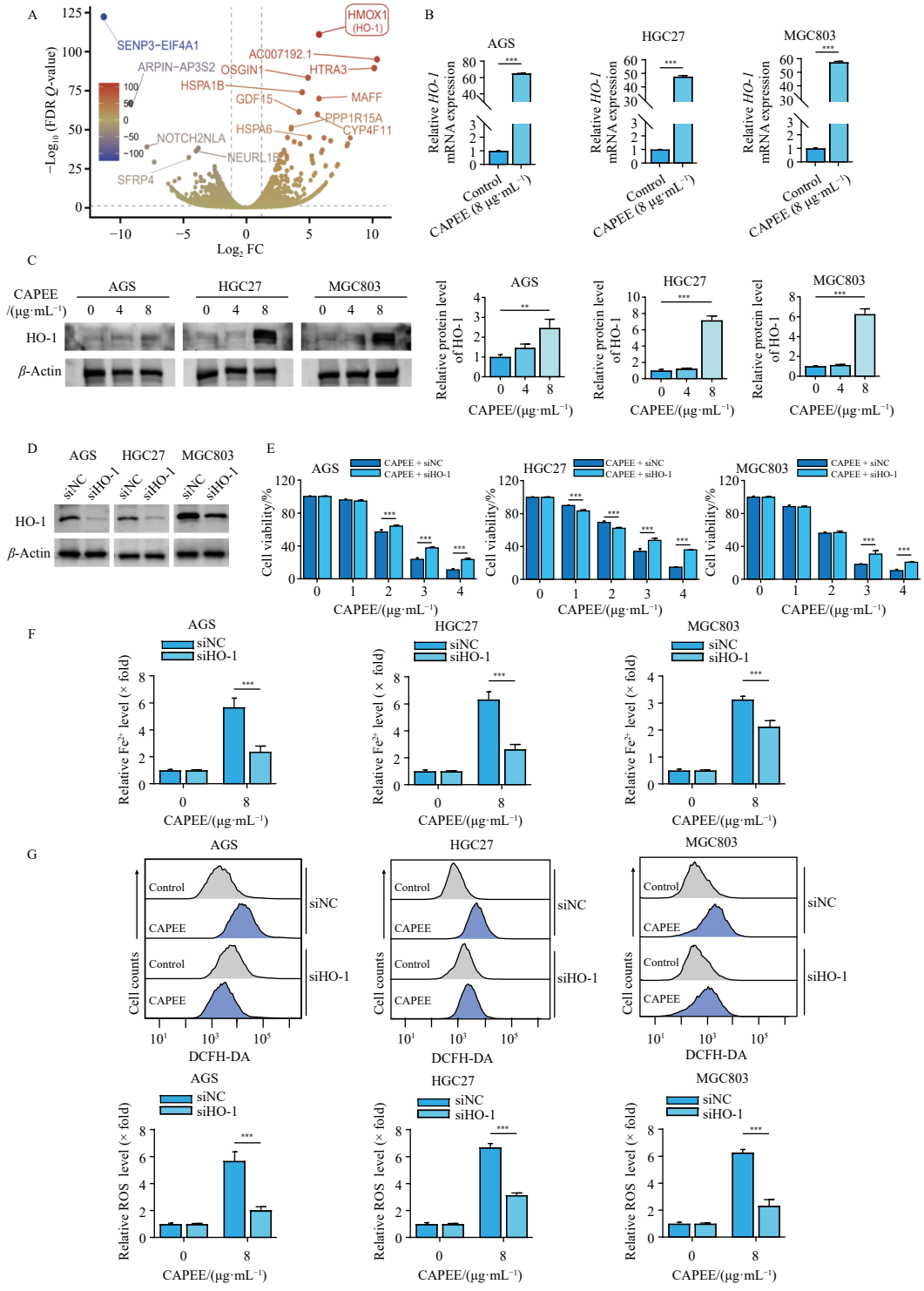

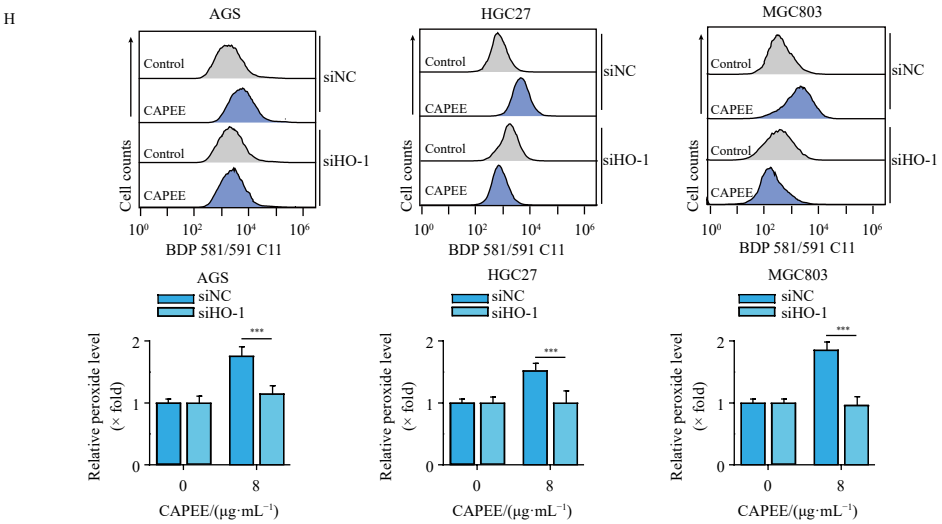

Fig. 5 HO-1 was involved in the induction of ferroptosis by CAPEE in human GC AGS, HGC27, and MGC803 cells. (A) HGC27 cells were exposed to 24 h of 0.8 μg·mL^{-1} CAPEE treatment. RNA-seq assay was carried out for mapping alterations of gene expression and comparing the changes in HO-1 expression (n = 3). (B) AGS, HGC-27, and MGC803 cells were exposed to 24 h of 0 or 8 μg·mL^{-1} CAPEE treatment. HO-1 mRNA expression was measured through qRT-PCR (n = 3). (C) AGS, HGC-27, and MGC803 cells were exposed to 48 h of 0, 4, or 8 μg·mL^{-1} CAPEE treatment. HO-1 protein expression in the cells was detected by immunoblotting (n = 3). Left panel: representative images; right panel: quantitative data. (D) The siRNAs targeting the HO-1 gene (siHO-1) and the control siRNAs (siNC) were transfected into human GC cells, followed by 48 h of incubation. HO-1 protein level was measured through immunoblotting (n = 3). (E) AGS, HGC27, and MGC803 cells transfected with siHO-1 or siNC were exposed to 72 h of 0, 1, 2, 3, or 4 μg·mL^{-1} CAPEE treatment. MTT assay was conducted to determine cell viability (n = 3). (F) AGS, HGC27, and MGC803 cells transfected with siHO-1 or siNC were exposed to 48 h of 0 or 8 μg·mL^{-1} CAPEE treatment. Fe^{2+} contents were measured (n = 3). (G) AGS, HGC27, and MGC803 cells transfected with siHO-1 or siNC were exposed to 48 h of 0 or 8 μg·mL^{-1} CAPEE treatment. ROS contents were detected (n = 3). Upper panel: representative images; lower panel: quantitative data. (H) AGS, HGC27, and MGC803 cells transfected with siHO-1 or siNC were exposed to 48 h of 0 or 8 μg·mL^{-1} CAPEE treatment. Lipid peroxide contents were analyzed (n = 3). Upper panel: representative images; lower panel: quantitative data. The results were expressed as mean ± SD. $^{*}P < 0.05$, $^{**}P < 0.01$, and $^{***}P < 0.001$.

G_0/G_1 phase. For instance, Picrasidine induces colon cancer cell cycle arrest in G_0/G_1 phase, thereby exhibiting anti-colon cancer properties [32]. Rutin demonstrates G_0/G_1 phase blockade in various cancer cells, including prostate, colon, and cervical cancer cells, manifesting anti-tumor effects [33]. The p21 protein, a member of the Cip/Kip family of cell cycle protein-dependent kinase inhibitors, and its regulated downstream proteins represent crucial targets for anti-cancer drug development [34]. Cyclin D1 forms a complex with CDK4, functioning as a critical regulator of cell cycle transition from G_1 to S phases [35]. Upon activation, p21 arrests tumor cells in G_1 phase through inhibition of cyclin/CDK complex expression [36]. The cell cycle blockade mediated by p21-cyclin/CDKs represents a fundamental molecular mechanism for numerous anti-tumor drugs. Pirfenidone enhances p21 expression and induces G_0/G_1 phase blockade in human pancreatic cancer cells by suppressing cyclin D/CDK4/6 complex expression [37]. Tumor cells typically exhibit genetic instability due to defective gene damage response, rendering them vulnerable, and drug-induced DNA damage represents a key anti-tumor strategy [38]. DNA damage constitutes the primary cause of cell cycle blockade [39]. Following DNA damage, p21 transcript levels increase significantly [40]. DHMMF, a flavonoid compound isolated from Chinese dragon's blood, induces DNA damage and elevates p21 expression, subsequently arresting cell cycle and demonstrating anti-hepatocellular carcinoma effects [41]. In this investigation, CAPEE arrested the cell cycle of human GC cells in G_0/G_1 phase. Furthermore, RT-qPCR and immunoblotting assays revealed that CAPEE enhanced p21 expression in human GC cells. Additionally, CAPEE suppressed cyclin D1/CDK4 signaling in human GC cells. Comet and immunoblotting assays demonstrated that CAPEE induced DNA damage within human GC cells. In conclusion, CAPEE may induce G_0/G_1 phase blockade of human GC cells through activation of the DNA damage-p21-cyclin D1/CDK4 signaling axis, thereby inhibiting human GC cell proliferation.

Ferroptosis represents an iron-dependent programmed type of cell death distinct from autophagy and apoptosis, characterized by iron-dependent oxidative stress. The accumulation of iron, release of free radicals, lipid peroxidation, and fatty acid production are crucial factors in ferroptosis induction [42]. Multiple tumor-related genes and pathways can regulate ferroptosis, and various anti-tumor drugs demonstrate efficacy through ferroptosis activation [43]. Consequently, the development of ferroptosis-targeting anti-tumor drugs presents significant potential. HO-1 functions as a rate-limiting enzyme in heme metabolism. Elevated HO-1 expression can trigger tumor cell death and suppress tumor growth [44]. HO-1 catalyzes heme's oxidative cleavage to produce equimolar CO, Fe^{2+}, and biliverdin, with accumulated Fe^{2+} generating ROS through the Fenton reaction. Additionally, HO-1 cleaves biliverdin to release substantial Fe^{2+}, leading to ROS accumulation and subsequent DNA damage or ferroptosis [45]. Quercetin administration enhances HO-1 protein levels and Fe^{2+} accumulation in GC cells, inducing ferroptosis and exhibiting anti-GC effects [46]. In osteosarcoma cells, mitochondrial ROS enhance HIF-1α expression, leading to HO-1 and Fe^{2+} overexpression, ROS accumulation, glutathione peroxidase depletion, and ferroptosis induction [47]. Moreover, β-elemene combined with cetuximab induces iron-dependent ROS accumulation, lipid peroxidation, and HO-1 upregulation in colorectal cancer cells [48]. Tagitin C increases ROS and lipid peroxidation through the endoplasmic reticulum stress-mediated PERK-Nrf2-HO-1 signaling pathway, inducing ferroptosis in human colorectal cancer cells [49]. Furthermore, abietic acid elevates ROS, intracellular iron, and malondialdehyde levels in bladder cancer cells, inducing ferroptosis by downregulating GPX4 and upregulating HO-1 [50]. This study demonstrates that CAPEE increases Fe^{2+} levels within human GC cells, triggering the Fenton reaction, leading to ROS accumulation and enhanced lipid peroxidation, thereby inducing ferroptosis. Additionally, transcriptome sequencing, RT-qPCR, immunoblotting, and immunohistochemical staining assays revealed CAPEE-induced HO-1 upregulation within human GC cells. RNA interference-mediated HO-1 knockdown significantly reduced CAPEE-induced increases in Fe^{2+}, ROS, and lipid peroxidation in human GC cells. In summary, CAPEE upregulates HO-1 expression, resulting in Fe^{2+} accumulation, increased ROS production, enhanced lipid peroxidation, and ferroptosis induction, thereby exerting anti-GC effects.

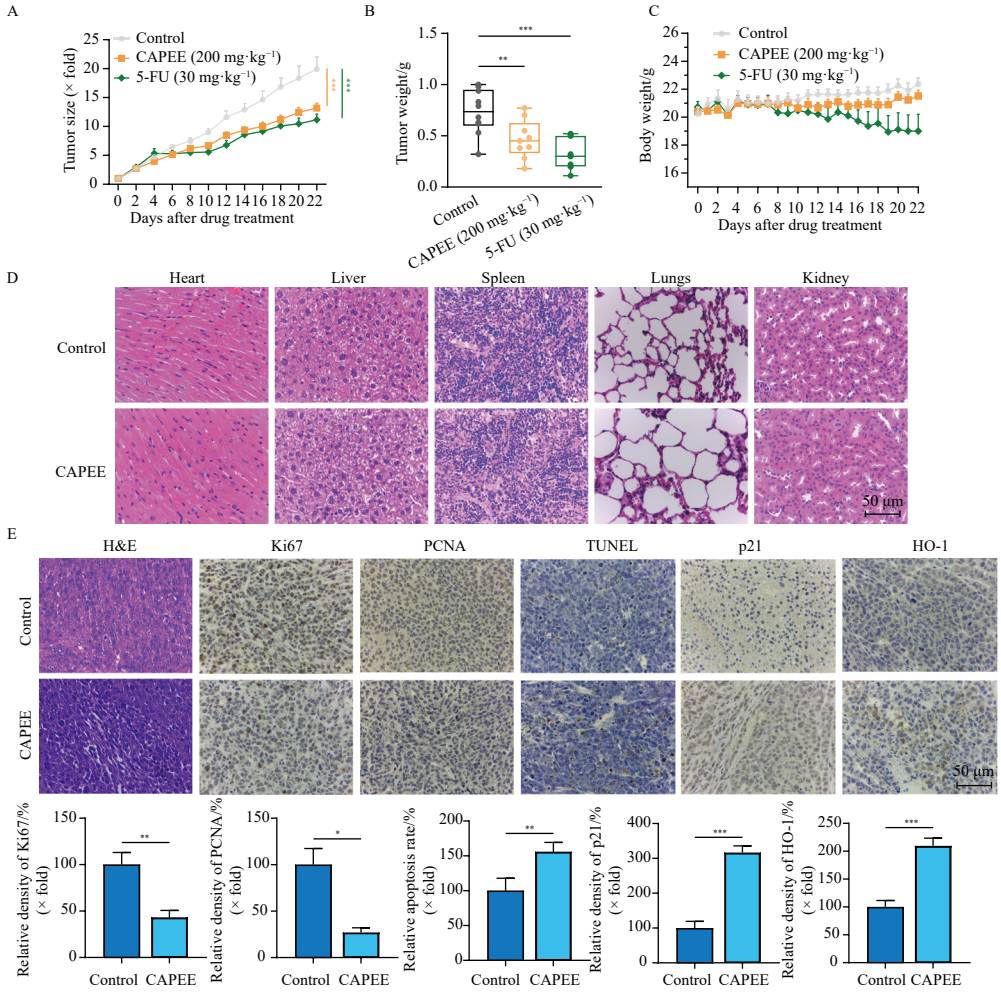

Fig. 6 Anti-gastric cancer effect of CAPEE *in vivo*. A nude mouse xenograft tumor model was constructed using human GC HGC27 cells and classified as 3 groups, namely, control group (double-distilled water solution containing 2.5% Tween 80, once a day, i.g.), the CAPEE administration group (200 mg·kg^{-1}, once/day, i.g.), and the 5-FU-positive group (30 mg·kg^{-1}, every other day, i.p.). Tumor volume growth curves of the mice (A), mouse tumor weight (B), and mouse body weight curves (C). n = 9 for each group. (D) H&E staining for the nude mouse liver, heart, spleen, kidney and lung tissues of CAPEE-treated and control groups (n = 3); scale bar: 50 μm. (E) Immunohistochemistry analysis for determining expression of Ki67, PCNA, p21, and HO-1 in tumor tissues of CAPEE-treated and control groups (n = 3). Upper panel: representative images; lower panel: quantitative data. scale bar: 50 μm. The results were expressed as mean ± SD. $^{*}P < 0.05$, $^{**}P < 0.01$, and $^{***}P < 0.001$.

5. Conclusion

In conclusion, this study presents the first report of CAPEE's anti-GC activity both *in vitro* and *in vivo*. The research reveals that the DNA damage-p21-cyclin D1/CDK4 axis potentially mediates CAPEE-induced cell cycle arrest in human GC cells. Furthermore, HO-1 upregulation-induced iron overload may facilitate CAPEE-induced ferroptosis in human GC cells. Thus, CAPEE represents a promising candidate drug for GC treatment through dual mechanisms of cell cycle arrest and ferroptosis induction. This comprehensive investigation of CAPEE's anti-GC effects at molecular, cellular, and animal levels provides potential therapeutic options for GC treatment and establishes a theoretical foundation for further research and clinical applications of Chinese agarwood's anti-GC properties. The findings contribute significantly to the rational development and utilization of Chinese agarwood in traditional Chinese medicine anti-tumor drug research. Future research will evaluate CAPEE's *in vivo* anti-GC activity using primary GC animal models, assess its efficacy and toxicity across various dosages, and isolate monomer components with significant anti-GC activity, potentially yielding new drug candidates or lead compounds for GC treatment. Additionally, RNA interference technology will be employed to provide robust evidence supporting CAPEE's anti-GC effects, particularly regarding cell cycle arrest induction through p21-cyclin D1/CDK4 signaling pathway regulation.

Funding

This work was supported by the Natural Science Foundation of Beijing City (No. J230034), the Fundamental Research Funds for the Central Universities (No. 2023-JYB-JBQN-051), and the Talent Cultivation Project of Beijing University of Chinese Medicine (No. JZPY202206).

Data availability statement

The data that support the findings of this study are available from the corresponding author upon reasonable request.

Declaration of competing interest

These authors have no conflict of interest to declare.

References

1 Sung H, Ferlay J, Siegel RL, et al. Global Cancer Statistics 2020: GLOBOCAN estimates of incidence and mortality worldwide for 36 cancers in 185 countries. *CA Cancer J Clin*. 2021;71(3):209-249. https://doi.org/10.3322/caac.21660.

2 Li K, Zhang A, Li X, et al. Advances in clinical immunotherapy for gastric cancer. *Biochim Biophys Acta Rev Cancer*. 2021;1876(2):188615. https://doi.org/10.1016/j.bbcan.2021.188615.

3 Wang S, Wang C, Peng D, et al. Agarwood essential oil displays sedative-

hypnotic effects through the GABAergic system. *Molecules*. 2017;22(12): 2190. https://doi.org/10.3390/molecules22122190.
4 Li W, Chen HQ, Wang H, et al. Natural products in agarwood and *Aquilaria* plants: chemistry, biological activities and biosynthesis. *Nat Prod Rep*. 2021;38(3):528-565. https://doi.org/10.1039/d0np00042f.
5 Hashim YZ, Kerr PG, Abbas P, et al. *Aquilaria* spp. (agarwood) as source of health beneficial compounds: a review of traditional use, phytochemistry and pharmacology. *J Ethnopharmacol*. 2016;189:331-360. https://doi.org/10.1016/j.jep.2016.06.055.
6 Shivanand P, Arbie NF, Krishnamoorthy S, et al. Agarwood-the fragrant molecules of a wounded tree. *Molecules*. 2022;27(11):3386. https://doi.org/10.3390/molecules27113386.
7 Hashim YZ, Phirdaous A, Azura A. Screening of anticancer activity from agarwood essential oil. *Pharmacognosy Res*. 2014;6(3):191-194. https://doi.org/10.4103/0974-8490.132593.
8 Dahham SS, Hassan LE, Ahamed MB, et al. *In vivo* toxicity and antitumor activity of essential oils extract from agarwood (*Aquilaria crassna*). *BMC Complement Altern Med*. 2016;16:236. https://doi.org/10.1186/s12906-016-1210-1.
9 Zhang H, Ma JL, Chang C, et al. Gastroprotective 2-(2-phenylethyl)chromone-sesquiterpene hybrids from the resinous wood of *Aquilaria sinensis* (Lour.) Gilg. *Bioorg Chem*. 2023;133:106396. https://doi.org/10.1016/j.bioorg.2023.106396.
10 Huo HX, Zhu ZX, Pang DR, et al. Anti-neuroinflammatory sesquiterpenes from Chinese eaglewood. *Fitoterapia*. 2015;106:115-121. https://doi.org/10.1016/j.fitote.2015.08.009.
11 Chen X, Zhao Y, Yang A, et al. Chinese Dragon's Blood EtOAc extract inhibits liver cancer growth through downregulation of Smad3. *Front Pharmacol*. 2020;11:669. https://doi.org/10.3389/fphar.2020.00669.
12 Hu Z, Wang Y, Huang F, et al. Brain-expressed X-linked 2 is pivotal for hyperactive mechanistic target of rapamycin (mTOR)-mediated tumorigenesis. *J Biol Chem*. 2015;290(42):25756-25765. https://doi.org/10.1074/jbc.M115.665208.
13 Jin F, Jiang K, Ji S, et al. Deficient TSC1/TSC2-complex suppression of SOX9-osteopontin-AKT signalling cascade constrains tumour growth in tuberous sclerosis complex. *Hum Mol Genet*. 2017;26(2):407-419. https://doi.org/10.1093/hmg/ddw397.
14 He M, Zhang G, Shen F, et al. Effects of Z-VaD-Ala-Asp-fluoromethyl ketone (Z-VAD-FMK) and acetyl-Asp-Glu-Val-Asp-aldehyde (Ac-DEVD-CHO) on inflammation and mucus secretion in mice exposed to cigarette smoke. *Int J Chron Obstruct Pulmon Dis*. 2023;18:69-78. https://doi.org/10.2147/copd.S385748.
15 McArthur K, Whitehead LW, Heddleston JM, et al. BAK/BAX macropores facilitate mitochondrial herniation and mtDNA efflux during apoptosis. *Science*. 2018;359:6378. https://doi.org/10.1126/science.aao6047.
16 Hershko C, Weatherall DJ. Iron-chelating therapy. *Crit Rev Clin Lab Sci*. 1988;26(4):303-345. https://doi.org/10.3109/10408368809105894.
17 Pedre B, Barayeu U, Ezeriņa D, et al. The mechanism of action of *N*-acetylcysteine (NAC): the emerging role of H_2S and sulfane sulfur species. *Pharmacol Ther*. 2021;228:107916. https://doi.org/10.1016/j.pharmthera.2021.107916.
18 Miotto G, Rossetto M, Di Paolo ML, et al. Insight into the mechanism of ferroptosis inhibition by ferrostatin-1. *Redox Biol*. 2020;28:101328. https://doi.org/10.1016/j.redox.2019.101328.
19 Wang X, Gao B, Liu X, et al. Salinity stress induces the production of 2-(2-phenylethyl)chromones and regulates novel classes of responsive genes involved in signal transduction in *Aquilaria sinensis* calli. *BMC Plant Biol*. 2016;16(1):119. https://doi.org/10.1186/s12870-016-0803-7.
20 Zhang X, Wang LX, Hao R, et al. Sesquiterpenoids in agarwood: biosynthesis, microbial induction, and pharmacological activities. *J Agric Food Chem*. 2024;72(42):23039-23052. https://doi.org/10.1021/acs.jafc.4c06383.
21 Wang S, Wang C, Yu Z, et al. Agarwood essential oil ameliorates restrain stress-induced anxiety and depression by inhibiting HPA axis hyperactivity. *Int J Mol Sci*. 2018;19(11):3468. https://doi.org/10.3390/ijms19113468.
22 Wang Y, Hussain M, Jiang Z, et al. *Aquilaria* species (Thymelaeaceae) distribution, volatile and non-volatile phytochemicals, pharmacological uses, agarwood grading system, and induction methods. *Molecules*. 2021;26(24): 7708. https://doi.org/10.3390/molecules26247708.
23 Xie Y, Song L, Li C, et al. Eudesmane-type and agarospirane-type sesquiterpenes from agarwood of *Aquilaria agallocha*. *Phytochemistry*. 2021;192:112920. https://doi.org/10.1016/j.phytochem.2021.112920.
24 Ye W, He X, Wu H, et al. Identification and characterization of a novel sesquiterpene synthase from *Aquilaria sinensis*: an important gene for agarwood formation. *Int J Biol Macromol*. 2018;108:884-892. https://doi.org/10.1016/j.ijbiomac.2017.10.183.
25 Wang S, Yu Z, Wang C, et al. Chemical constituents and pharmacological activity of agarwood and *Aquilaria* plants. *Molecules*. 2018;23(2):342. https://doi.org/10.3390/molecules23020342.
26 Dahham SS, Tabana YM, Iqbal MA, et al. The anticancer, antioxidant and antimicrobial properties of the sesquiterpene *β*-caryophyllene from the essential oil of *Aquilaria crassna*. *Molecules*. 2015;20(7):11808-11829. https://doi.org/10.3390/molecules200711808.
27 Huang XL, Cai D, Gao P, et al. Aquilariperoxide A, a sesquiterpene dimer from agarwood of *Aquilaria sinensis* with dual antitumor and antimalarial rffects. *J Org Chem*. 2023;88(13):8352-8359. https://doi.org/10.1021/acs.joc.3c00372.
28 Morana O, Wood W, Gregory CD. The apoptosis paradox in cancer. *Int J Mol Sci*. 2022;23(3):1328. https://doi.org/10.3390/ijms23031328.
29 Pistritto G, Trisciuoglio D, Ceci C, et al. Apoptosis as anticancer mechanism: function and dysfunction of its modulators and targeted therapeutic strategies. *Aging (Albany NY)*. 2016;8(4):603-619. https://doi.org/10.18632/aging.100934.
30 Kayagaki N, Webster JD, Newton K. Control of cell death in health and disease. *Annu Rev Pathol*. 2024;19:157-180. https://doi.org/10.1146/annurev-pathmechdis-051022-014433.
31 Hidalgo M, Rowinsky EK. The rapamycin-sensitive signal transduction pathway as a target for cancer therapy. *Oncogene*. 2000;19(56):6680-6686. https://doi.org/10.1038/sj.onc.1204091.
32 Liu J, Guo Y, Cao J. Matrine triggers colon cancer cell apoptosis and G_0/G_1 cell cycle arrest *via* mediation of microRNA-22. *Phytother Res*. 2020;34(7):1619-1628. https://doi.org/10.1002/ptr.6626.
33 Khan F, Pandey P, Upadhyay TK, et al. Anti-cancerous effect of rutin against HPV-C33A cervical cancer cells *via* G_0/G_1 cell cycle arrest and apoptotic induction. *Endocr Metab Immune Disord Drug Targets*. 2020;20(3):409-418. https://doi.org/10.2174/1871530319666190806122257.
34 Chen J, Amos CI, Merriman KW, et al. Genetic variants of p21 and p27 and pancreatic cancer risk in non-Hispanic Whites: a case-control study. *Pancreas*. 2010;39(1):1-4. https://doi.org/10.1097/MPA.0b013e3181bd51c8.
35 Goel S, DeCristo MJ, McAllister SS, et al. CDK4/6 Inhibition in cancer: beyond cell cycle arrest. *Trends Cell Biol*. 2018;28(11):911-925. https://doi.org/10.1016/j.tcb.2018.07.002.
36 Shamloo B, Usluer S. p21 in cancer research. *Cancers (Basel)*. 2019;11(8): 1178. https://doi.org/10.3390/cancers11081178.
37 Usugi E, Ishii K, Hirokawa Y, et al. Antifibrotic agent pirfenidone suppresses proliferation of human pancreatic cancer cells by inducing G_0/G_1 cell cycle arrest. *Pharmacology*. 2019;103(5-6):250-256. https://doi.org/10.1159/000496831.
38 Ricciuti B, Recondo G, Spurr LF, et al. Impact of DNA damage response and repair (DDR) gene mutations on efficacy of PD-L1 immune checkpoint inhibition in non-small cell lung cancer. *Clin Cancer Res*. 2020;26(15):4135-4142. https://doi.org/10.1158/1078-0432.Ccr-19-3529.
39 Brown JS, O'Carrigan B, Jackson SP, et al. Targeting DNA repair in cancer: beyond PARP inhibitors. *Cancer Discov*. 2017;7(1):20-37. https://doi.org/10.1158/2159-8290.Cd-16-0860.
40 Kozyrska K, Pilia G, Vishwakarma M, et al. p53 directs leader cell behavior, migration, and clearance during epithelial repair. *Science*. 2022;375(6581): eabl8876. https://doi.org/10.1126/science.abl8876.
41 Tian Y, Wang L, Chen X, et al. DHMMF, a natural flavonoid from Resina Draconis, inhibits hepatocellular carcinoma progression *via* inducing apoptosis and G_2/M phase arrest mediated by DNA damage-driven upregulation of p21. *Biochem Pharmacol*. 2023;211:115518. https://doi.org/10.1016/j.bcp.2023.115518.
42 Wang D, Tang L, Zhang Y, et al. Regulatory pathways and drugs associated with ferroptosis in tumors. *Cell Death Dis*. 2022;13(6):544. https://doi.org/10.1038/s41419-022-04927-1.
43 Dolma S, Lessnick SL, Hahn WC, et al. Identification of genotype-selective antitumor agents using synthetic lethal chemical screening in engineered human tumor cells. *Cancer Cell*. 2003;3(3):285-296. https://doi.org/10.1016/s1535-6108(03)00050-3.
44 Chiang SK, Chen SE, Chang LC. A dual role of heme oxygenase-1 in cancer cells. *Int J Mol Sci*. 2018;20(1):39. https://doi.org/10.3390/ijms20010039.
45 Tang Z, Ju Y, Dai X, et al. HO-1-mediated ferroptosis as a target for protection against retinal pigment epithelium degeneration. *Redox Biol*. 2021;43: 101971. https://doi.org/10.1016/j.redox.2021.101971.
46 Ding L, Dang S, Sun M, et al. Quercetin induces ferroptosis in gastric cancer cells by targeting SLC1A5 and regulating the p-Camk2/p-DRP1 and NRF2/GPX4 axis. *Free Radic Biol Med*. 2024;213:150-163. https://doi.org/10.1016/j.freeradbiomed.2024.01.002.
47 Lu C, Zhang Z, Fan Y, et al. Shikonin induces ferroptosis in osteosarcomas through the mitochondrial ROS-regulated HIF-1α/HO-1 axis. *Phytomedicine*. 2024;135:156139. https://doi.org/10.1016/j.phymed.2024.156139.
48 Chen P, Li X, Zhang R, et al. Combinative treatment of *β*-elemene and cetuximab is sensitive to KRAS mutant colorectal cancer cells by inducing ferroptosis and inhibiting epithelial-mesenchymal transformation. *Theranostics*. 2020;10(11):5107-5119. https://doi.org/10.7150/thno.44705.
49 Wei R, Zhao Y, Wang J, et al. Tagitinin C induces ferroptosis through PERK-Nrf2-HO-1 signaling pathway in colorectal cancer cells. *Int J Biol Sci*. 2021;17(11):2703-2717. https://doi.org/10.7150/ijbs.59404.
50 Xu Y, Tong Y, Lei Z, et al. Abietic acid induces ferroptosis *via* the activation of the HO-1 pathway in bladder cancer cells. *Biomed Pharmacother*. 2023;158: 114154. https://doi.org/10.1016/j.biopha.2022.114154.